

Sub-Newtonian coalescence in polymeric fluids

Abhineet Singh Rajput,[†] Sarath Chandra Varma,[†] and Alope Kumar^{*,†}

[†]*Department of Mechanical Engineering, Indian Institute of Science, Bangalore, India*

E-mail: *alokekumar@iisc.ac.in

Abstract

We present a theoretical framework for capturing the coalescence of a pendant drop with a sessile drop in polymeric fluids. The framework is based on the unification of various constitutive laws under high Weissenberg creeping flow limit. Our results suggest that the phenomenon comes under a new regime namely, the sub-Newtonian regime followed by the limiting case of arrested coalescence with the arrest angle $\theta_{arrest} \propto Ec^{-1/2}$, where Ec is the Elasto-capillary number. Further, we propose a new time scale T^* integrating the continuum variable Ec and the macromolecular parameter N_e , the entanglement density to describe the liquid neck evolution. Finally, we validate the framework with high speed imaging experiments performed across different molecular weights of Poly(ethylene oxide) (PEO).

Introduction

Coalescence is an energy minimization phenomenon in which two drops merge to form a thermodynamically stable daughter drop.¹ Coalescence of droplets of Newtonian fluids plays a key role in rain drop condensation,^{2,3} combustion,⁴ atomization of metal droplets;⁵ while non-Newtonian fluid droplets coalescence finds applications in food industry,⁶ spray coating and paintings,^{7,8} even processes linked to life like those in growth and development of tumor.⁹

Despite the varied and versatile application of non-Newtonian fluids, coalescence dynamics of such fluids remains a sparsely studied area. The vastness of the domain of non-Newtonian fluids - they can range from macromolecular fluids to various colloids - makes a unified understanding even more elusive. Each subclass has a different micro-structure composition leading to distinct behaviors. However, there are few recent studies on a special class of non-Newtonian fluids i.e macromolecular fluids¹⁰⁻¹⁴ that have highlighted the deviation from proposed Newtonian behaviour. But a generalized theoretical framework unifying various constitutive laws to probe the phenomenon in viscoelastic fluids remains an open question.

Recent study by Chen et al.¹⁴ on a subclass of viscoelastic fluids i.e polymers and gels showed that at late time scales coalescence is slower than the Newtonian drops. This conclusion was drawn based on stress relaxation behaviour in polymers using molecular dynamics simulation. Similarly Xu et al.¹⁵ also reported a slower growth of neck during coalescence of two immiscible Newtonian droplets. Another study, which employed numerical experiments on sessile-sessile drop coalescence of power-law fluids, showed a deviation from Newtonian behaviour as a function of the power-law exponent.¹⁶ Our previous study on polymeric droplet coalescence¹² highlighted the relevance of macromolecular relaxation time on the neck radius evolution R . The schematic of the neck during coalescence is shown in Fig. 1(a). Instead of viscous versus inertial regime delineation in Newtonian fluids, aqueous solutions of macromolecules showed three different regimes namely, inertio-elastic, viscoelastic and elasticity dominated regimes. The non-dimensional parameter concentration ratio, c/c^* , governed the appearance of the various regimes. It has also been shown that the temporal evolution of the bridge follows a universal behaviour in inertio-elastic and viscoelastic regimes i.e $R \sim t^b$ (where, b is power-law exponent) with $b = 0.37$ along with continuously decreasing b in the elasticity dominated regime. Based on scaling analysis using linear Phan-Thein-Tanner (PTT)^{17,18} constitutive equation the study proposed a time scale $\tau^* = \sqrt{\frac{\eta\lambda}{\rho R_o^2}}$ where η , ρ and R_o are the viscosity, density and length scale of the polymeric droplet to capture neck evolution exponent b . Whether these deviations from Newtonian behaviour in macromolecular

fluids is due to visco-elasticity or shear dependent viscosity remains unresolved.

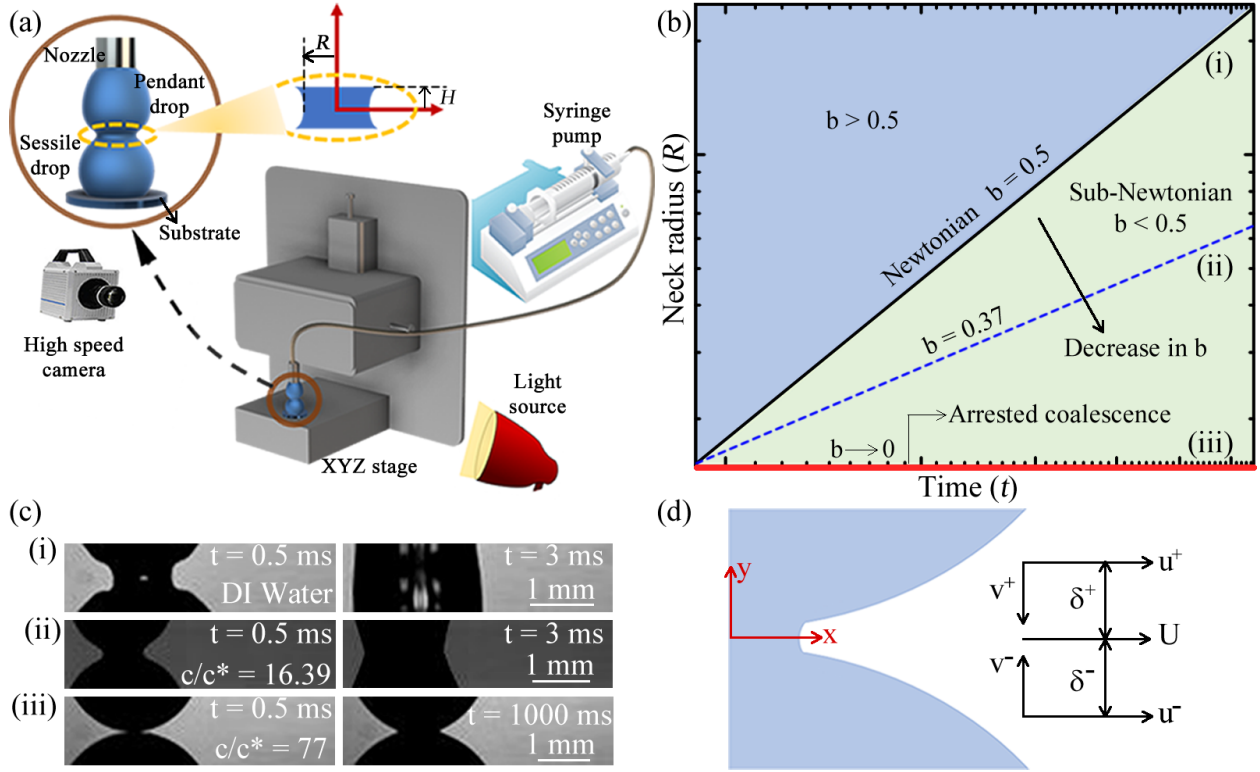


Figure 1: (a) Schematic of experimental setup showing the geometric parameters neck radius R and semi-bridge height H , (b) Regime map showing the classification of coalescence based on power-law exponent b . (c) Snapshots showing the neck at different time instants for (i) DI water, (ii) $c/c^* = 16.39$ of PEO $M_w = 5 \times 10^6$ g/mol and (iii) $c/c^* = 77$ PEO $M_w = 1 \times 10^5$ g/mol indicating the Newtonian, sub-Newtonian and arrested coalescence respectively, (d) Schematic of velocity distribution at the neck region for sessile-pendant coalescence.

In the current study, we have developed a theoretical model to capture the neck radius evolution across different regimes. The theoretical framework is developed based on the unification of Oldroyd-B, linear PTT, Giesekus constitutive equations¹⁹ under high Weissenberg number Wi creeping flow limit. Thus this resolves the unanswered argument that visco-elasticity is the reason for deviation in neck evolution dynamics. However, for simplicity we use Giesekus constitutive equation²⁰ to explain the model. The proposed model is validated with the experiments performed with Poly(ethylene oxide) (PEO) for a range of molecular weights M_w . Apart from the theoretical model, we have also demonstrated the effect of entanglement density N_e on coalescence to propose a new time scale T^* that intertwines

continuum and molecular approaches to macromolecular fluid. Using the analogy of sub-diffusive behavior in Brownian dynamics, we name this broader class of sluggish merging of two droplets as sub-Newtonian coalescence. For the sessile-pendant droplet configuration, the regime of sub-Newtonian coalescence is marked by a power-law exponent (b) such that $0 < b < 0.5$. The right-hand limit corresponds to a purely viscous Newtonian fluid, whereas the left-hand limit corresponds to arrested-coalescence. Macromolecular fluids coalescence are such examples of sub-Newtonian coalescence where the presence of an additional resistance by elastic force slows down the coalescence resulting in an exponent b lesser than the universal $b = 0.5$ for Newtonian fluids. Even in Newtonian droplet coalescence, if the drops are immiscible one sees sub-Newtonian coalescence. Further we also propose a theoretical limit for an arrested coalescence ($b \rightarrow 0$). A regime map delineating the Newtonian ($b = 0.5$), sub-Newtonian ($b < 0.5$) and the arrested coalescence ($b \rightarrow 0$) is shown in Fig. 1(b) with the blue dashed line representing the universality proposed for the polymeric fluids in our previous study¹⁰ and the solid red line signifying the arrested limit. Fig. 1(c) represents the snapshots of the phenomenon at different time instants for DI water, $c/c^* = 16.39$ of PEO $M_w = 5 \times 10^6$ g/mol and 77 of PEO $M_w = 1 \times 10^5$ g/mol respectively. It can be observed from Fig. 1(b) that the neck evolution slows down as one moves from Newtonian to sub-Newtonian with the limiting case being the arrested coalescence. A detailed discussion on arrested coalescence is presented in the later sections.

Theory

To obtain the theoretical solution for coalescence phenomenon, we employ the symmetry of the problem and formulate our analysis in two dimensional Cartesian coordinates as shown in Fig. 1(d). The kinematics of the flow is assumed to be quasi-radial at the neck region $y = 0$ implying that $u \neq 0$ and $v = 0$. For a small region of width δ on either sides of $y = 0$ line the flow field is such that $u^+ = u^- \neq 0$ and $v^+ = -v^- \neq 0$ respectively. Owing to the fact of mirror symmetry and quasi-radial assumption, the flow field at $y = 0$ line has the constraints

of $\frac{\partial u}{\partial y} = 0$ and $\frac{\partial v}{\partial x} = 0$.

The dynamics of the coalescence phenomenon is governed by conservation of mass and momentum equations along $y = 0$ line as shown in Eq (2) and Eq (3a-b). To get stress tensor $\boldsymbol{\tau}$ in Eq (3) we employ to Giesekus constitutive equation represented in Eq (4).

$$\frac{\partial u}{\partial x} + \frac{\partial v}{\partial y} = 0 \quad (1)$$

$$\rho \left(u \frac{\partial u}{\partial x} \right) = -\frac{\partial p}{\partial x} + \frac{\partial \tau_{xx}}{\partial x} + \frac{\partial \tau_{xy}}{\partial y} \quad (2a)$$

$$0 = -\frac{\partial p}{\partial y} + \frac{\partial \tau_{yy}}{\partial y} \quad (2b)$$

where, $\overset{\nabla}{\boldsymbol{\tau}} = \frac{\partial \boldsymbol{\tau}}{\partial t} + \mathbf{v} \cdot \nabla \boldsymbol{\tau} - (\nabla \mathbf{v}) \boldsymbol{\tau} - \boldsymbol{\tau} (\nabla \mathbf{v})^T$ is upper convected derivative.

By introducing the non-dimensional variables: $\mathbf{v}^* = \mathbf{v}/U$, $x^* = x/L$, $y^* = y/L$, $t^* = t/T$, $\boldsymbol{\tau}^* = \boldsymbol{\tau}/\boldsymbol{\tau}_c$, where $T := L/U$, U , L , $\boldsymbol{\tau}_c$ are the characteristic time, velocity, length and stress respectively, Eq (4) is reduced to different forms as proposed in literature.^{10,12} Based on the dominant scale of $\boldsymbol{\tau}_c$ the constitutive law can be reduced to three distinct regimes, namely viscous dominant regime ($\boldsymbol{\tau}_c = \frac{\eta U}{L}$), viscoelastic regime ($\boldsymbol{\tau}_c = Wi \frac{\eta U}{L}$) where, $Wi = \frac{\lambda U}{L}$ is Weissenberg number and elasticity dominant regime ($\boldsymbol{\tau}_c = \frac{\eta}{\lambda}$). Recently Varma et al.¹² used the scale ($\boldsymbol{\tau}_c = \frac{\eta}{\lambda}$) in elasticity dominated regime to predict the behaviour of b during coalescence. For inertio-elastic and viscoelastic regimes a semi-analytical model is proposed by Varma et al.¹⁰ in which the upper convected derivative in Eq (4) was dropped. However, that approximation is not valid in the elasticity dominated regime as the Reynolds number $Re = \frac{\rho U L}{\eta_o}$ is $\mathcal{O}(10^{-5})$ and Weissenberg number Wi is $\mathcal{O}(10^3)$ as shown in our previous study¹³ indicating that the flow has low Re and high Wi . A detailed discussion on the Re and Wi for the present study is given in results and discussion section. For low Re and high Wi flows, the upper convective derivative of stress in the constitutive equation is

the dominant term in Eq (3) (See supplementary information for the detailed derivation). Similarly, Renardy²¹ showed that the upper convected derivative in the various constitutive equations¹⁹ like Maxwell, Oldroyd-B, Linear PTT, exponential PTT model is the dominant term under quasi-steady assumption at high Wi and low Re . As the upper convective derivative is the predominant term, the present theory is independent of continuum based constitutive equations.

$$\tau_c \boldsymbol{\tau}^* + \frac{\tau_c \lambda U}{L} \left(\frac{\partial \boldsymbol{\tau}^*}{\partial t^*} + \overset{\nabla}{\boldsymbol{\tau}}^* + \frac{\alpha \tau_c L}{\eta U} \boldsymbol{\tau}^* \boldsymbol{\tau}^* \right) = 2 \frac{\eta U}{L} \mathbf{D}^* \quad (3)$$

$$\overset{\nabla}{\boldsymbol{\tau}}^* = 2\mathbf{D}^*. \quad (4)$$

As the coalescence phenomenon is predominately extensional, both the upper and lower convected derivative can be used to model the physics.²² In the present analysis, we have used the lower convected derivative $\overset{\Delta}{\boldsymbol{\tau}}^* = \frac{\partial \boldsymbol{\tau}}{\partial t} + \mathbf{v} \cdot \nabla \boldsymbol{\tau} + (\nabla \mathbf{v}) \boldsymbol{\tau} + \boldsymbol{\tau} (\nabla \mathbf{v})^T$. For capturing the neck evolution dynamics, stress tensor in Eq (5) is simplified for the spatial region $y = 0$ under the quasi-steady and quasi-radial assumptions to Eq (6a-c). The individual components of stress tensor are obtained by integrating Eq (6a-c) along $y = 0$ line as represented in Eq (7a-c).

$$u \frac{\partial \tau_{xx}}{\partial x} + 2\tau_{xx} \frac{\partial u}{\partial x} = 2 \frac{\eta}{\lambda} \frac{\partial u}{\partial x} \quad (5a)$$

$$u \frac{\partial \tau_{yy}}{\partial x} - 2\tau_{yy} \frac{\partial u}{\partial x} = -2 \frac{\eta}{\lambda} \frac{\partial u}{\partial x} \quad (5b)$$

$$u \frac{\partial \tau_{xy}}{\partial x} = 0 \quad (5c)$$

$$\tau_{xx} = \frac{\eta}{\lambda} + H/u^2 \quad (6a)$$

$$\tau_{xy} = M \quad (6b)$$

$$\tau_{yy} = \frac{\eta}{\lambda} + Fu^2 \quad (6c)$$

Here, H, M and F are integrating constants which in general are functions of y locally.

To get the semi-analytical solution for the neck evolution, the momentum equation Eq (3) is further simplified to Eq (8) by introducing the scaling arguments $u \sim U$, $x \sim R$, $y \sim \frac{R^2}{2R_o}$, $\frac{\partial p}{\partial x} \sim \sigma \left(\frac{1}{R^2} + \frac{2R_o}{R^3} \right)^{2/3}$ along with the components of stress tensor in Eq (3a-b) as $\frac{\partial \tau_{xx}}{\partial x} \sim \frac{\tau_{xx}}{R}$ and $\frac{\partial \tau_{xy}}{\partial y} \sim \frac{\tau_{xy}}{\frac{R^2}{2R_o}}$ (R_o is droplet radius). Here, Eq (8) is a bi-quadratic equation of the form given in Eq (9) in which A_1, A_2 and A_3 are scaling constants. Eq (9) has 4 solutions in which two are negative and two are positive. However, the negative solutions are physically irrelevant as they suggest the neck collapses with time. Among the two acceptable solutions $\sqrt{\frac{P}{2} + \sqrt{\frac{P^2}{4} + Q}}$ captures the physical scenario. Therefore, the acceptable solution of Eq (9) is of the form Eq (10) where $U = \frac{dR}{dt}$.

$$U^4 - \left(\frac{A_1 \sigma}{\rho} \left(\frac{1}{R} + \frac{2R_o}{R^2} \right) + \frac{A_2 \eta}{\rho \lambda} + \frac{2A_3 R_o}{\rho R} \right) U^2 - \frac{A_2}{\rho} = 0 \quad (7)$$

$$U^4 - P(\sigma, \rho, \eta, \lambda, R, R_o, A_1, A_2, A_3) U^2 - Q(A_2, \rho) = 0 \quad (8)$$

$$\frac{dR}{dt} = \sqrt{\frac{P}{2} + \sqrt{\frac{P^2}{4} + Q}} \quad (9)$$

Eq (10) is solved using first order finite difference scheme, in which time step Δt is taken sufficiently small to ensure numerical stability.

Results and Discussion

Once the droplets touch each other, neck begins to grow for attaining the thermodynamic equilibrium state of a single daughter droplet. This neck growth is characterised by the temporal evolution of neck radius R and semi-bridge height H as represented in Fig. 1(a). This evolution of neck radius at different time instants for concentration ratios c/c^* 12.31 and 24.32 of $M_w = 6 \times 10^5$ g/mol are shown in Fig. S1(a) and (b) respectively. Details of the experimental procedure is given in supplementary information.

Neck radius evolution for various concentrations ratios of $M_w = 1 \times 10^5$ and 6×10^5 g/mol is shown in Fig. 2(a). The data represented for all the concentration ratios is of an average of 5 trials. It can be observed from Fig. 2(a) that the neck radius evolution follows a power-law behaviour¹⁰ $R = at^b$ in the region of interest (ROI) along with decrease in power-law exponent b with c/c^* which is consistent with our previous study.¹² The error in measurement of b is less than $\pm 5\%$.

To interpret the neck evolution during coalescence of polymeric droplets it is essential to outline the underlying forces. These are elastic force F_e , viscous force F_v , inertial force F_i and capillary force F_c , where F_c drives the phenomenon while the other three resist it. The relative magnitudes of these resistive forces are captured by Reynolds number $Re = \langle \frac{\rho UL}{\eta_o} \rangle$, Weissenberg number $Wi = \langle \frac{\lambda U}{L} \rangle$, Elasticity number $El = Wi/Re$ where $U \sim \partial R/\partial t$ and $L \sim R^2/2R_o$ are the characteristic scales associated with the flow. The variation of Re and Wi with c/c^* is shown in Fig. 2(b) with delineation based on the regimes proposed in our previous study¹²(inertio-elastic (IE), viscoelastic (VE) and elasticity dominated (ED) regimes) for $M_w = 1 \times 10^5$ and $M_w = 6 \times 10^5$ g/mol along with the $M_w = 5 \times 10^6$ g/mol. Fig. 2(b) reveals that $Re < \mathcal{O}(10^{-2})$ and $Wi > \mathcal{O}(10^0)$ for $M_w = 1 \times 10^5$ and $M_w = 6 \times 10^5$ g/mol indicating the flow has low Re and high Wi .

In order to determine the closure to the analytical solution it is essential to study the physical behaviour of scaling parameters A_1, A_2 and A_3 represented in Eq (8). Among these scaling parameters, A_1 is the coefficient of capillary force that drives the coalescence dynamics

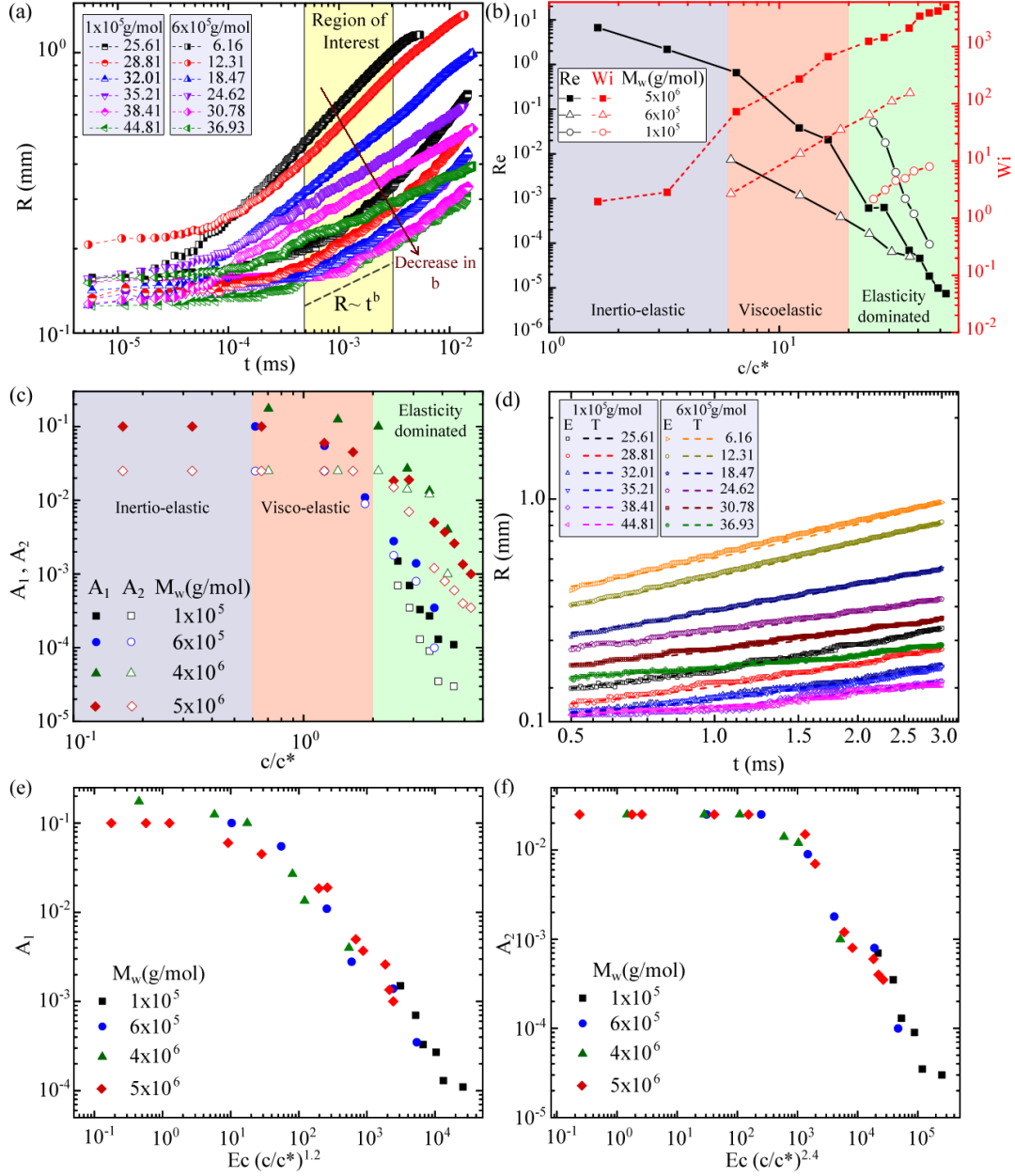


Figure 2: (a) Growth in neck radius for various concentration ratios c/c^* of PEO solutions showing the decrease in slope b for $M_w = 1 \times 10^5$ g/mol and $M_w = 6 \times 10^5$ g/mol, (b) Regime map showing the variation of Re and Wi with c/c^* across the molecular weight. (Note: Data for $M_w = 5 \times 10^6$ is obtained from our previous study¹³), (c) Dependence of scaling constants A_1 and A_2 on c/c^* for various molecular weights across various regimes, namely, Inertio-elastic, visco-elastic and elasticity dominated regimes. (Note: A_2 values represented are the magnitudes), (d) Agreement between the experiments and solution of Eq (10) for various c/c^* of $M_w = 1 \times 10^5$ g/mol and $M_w = 6 \times 10^5$ g/mol. Collapsing of scaling constants across molecular weights representing the dependence on Ec for (e) A_1 and (f) A_2 in which c/c^* is added empirically. (Note: A_2 values represented are the magnitudes).

while A_2 and A_3 are the coefficients of axial stress τ_{xx} and shear stress τ_{xy} respectively that oppose the neck growth. Owing to this nature, the coefficients A_2 and A_3 will have negative values while A_1 will have positive values. The magnitude of A_1 and A_2 used to get the numerical solution for all the chosen molecular weights with c/c^* are given in Fig. 2(c). It is observed numerically that Eq (10) has least sensitivity to A_3 , so we have assumed $A_3 = A_2$ without loss of any generality. Fig. 2(c) delineates the variation of A_1 and A_2 in IE, VE and ED regimes showing the constant values in IE and VE with a continuous decrease in ED regime.

The neck evolution represented in ROI of Fig. 2(a) is validated by numerically solving the proposed Eq (10) using the values of A_1 and A_2 given in Fig. 2(c). Fig. 2(d) shows the good agreement between the experiments and the proposed theory for $M_w = 1 \times 10^5$ and $M_w = 6 \times 10^5$ g/mol . To validate our theory further, the agreement between the present theory and the experimental results obtained from our previous study¹² for $M_w = 5 \times 10^6$ and $M_w = 4 \times 10^6$ g/mol is shown in Fig. S2 (a) and (b). The power-law exponent b obtained by fitting the experimental and the numerical data are given in Table-S1 (supplementary information) as b and b_{theo} respectively where b_{theo} is power-law exponent obtained from the fitting of theoretical data.

These scaling constants have a strong dependence on Elasto-capillary number $Ec = \frac{\text{Elastic Force}}{\text{Capillary Force}} = \frac{\eta_o R_o}{\sigma \lambda}$. By observing the dependence of A_1 and A_2 on Ec , c/c^* is added empirically in the form of $(c/c^*)^{1.2}$ and $(c/c^*)^{2.4}$ respectively to unify the functional form over different molecular weights as shown in Fig. 2(e) and Fig. 2(f) respectively. It is observed numerically that b_{theo} has strong dependence on A_1 . This is expected as A_1 is the coefficient of capillary forces that drive the coalescence dynamics. The parameter A_1 in Eq (8) corresponds to the relative contribution of capillary forces during the neck growth. It has been observed from our previous experiments¹² that, as the elasticity of droplets increases, the curvature of neck formed during coalescence changes, leading to an increase in capillary forces. Therefore, the term corresponding to A_1 in Eq (8) increases in magnitude. In or-

der to maintain an overall balance in Eq (8), the coefficient A_1 decreases. As A_1 needs to account for the capillary forces, it has a strong functional dependence on Ec which can be observed in Fig. 2(e). It can be noted from Fig. 2(e) that A_1 has a nearly constant value till $Ec(c/c^*)^{1.2} \sim O(10^0)$ and then it decreases as the elastic forces increase. This is also the signature of the presence of three different regimes in coalescence where the exponent b is constant in the IE/VE regime and a function of relaxation time λ in the ED regime.¹² Similarly the scaling parameters A_2 and A_3 are the coefficients of stress contributions in Eq (8) representing the relative contribution of elastic force and viscous force. As shown in Fig. 2(f), these parameters are almost constant for the value of $Ec(c/c^*)^{2.4} \sim O(10^2)$ followed by a strong decrease with increase in $Ec(c/c^*)^{2.4}$. It is further explained by Fig. 2(f), as a transition in coalescence regime from IE/VE to ED regime. As we move towards the elasticity dominated regime, the value of $Ec(c/c^*)^{2.4}$ increases owing to higher elasticity of droplets. This increase in elasticity of droplets increases the stress contributions in Eq (8). Therefore, to retain the balance in equation, parameters A_2 and A_3 decrease monotonically.

The power-law exponent b is the signature of the dominant governing force in coalescence dynamics. Apart from the early time scale where the exponent value is unity, it has a regime-dependent value for later time scales. For Newtonian, it is a universal value of $b = 0.5$,²³⁻²⁵ while for polymeric droplets, it is $b \leq 0.38$.¹⁰ This reduction in evolution exponent results from an additional resistance offered by elastic forces that slows the neck evolution thereby delaying coalescence. This sluggish merging of the two polymeric droplets owing to fluid elasticity is analogous to slowed diffusion of Brownian particles in viscoelastic media where diffusive exponent α less than unity in $\langle \Delta r^2 \rangle \propto t^\alpha$ marks the sub-diffusive regime.²⁶ And therefore, polymeric droplet coalescence can equivalently be classified as an example of a border class of coalescence with $b < 0.5$ which we name as the sub-Newtonian coalescence. Our previous study on sub-Newtonian type coalescence (Rheocoalescence)¹² showed, power-law exponent b depends on $\tau^* = \sqrt{\frac{\eta_0 \lambda}{\rho R_0^2}}$ (ratio of relaxation time and the Newtonian time scale). The corresponding dependence of b for $M_w = 6 \times 10^5$ and $M_w = 1 \times 10^5$ g/mol along with

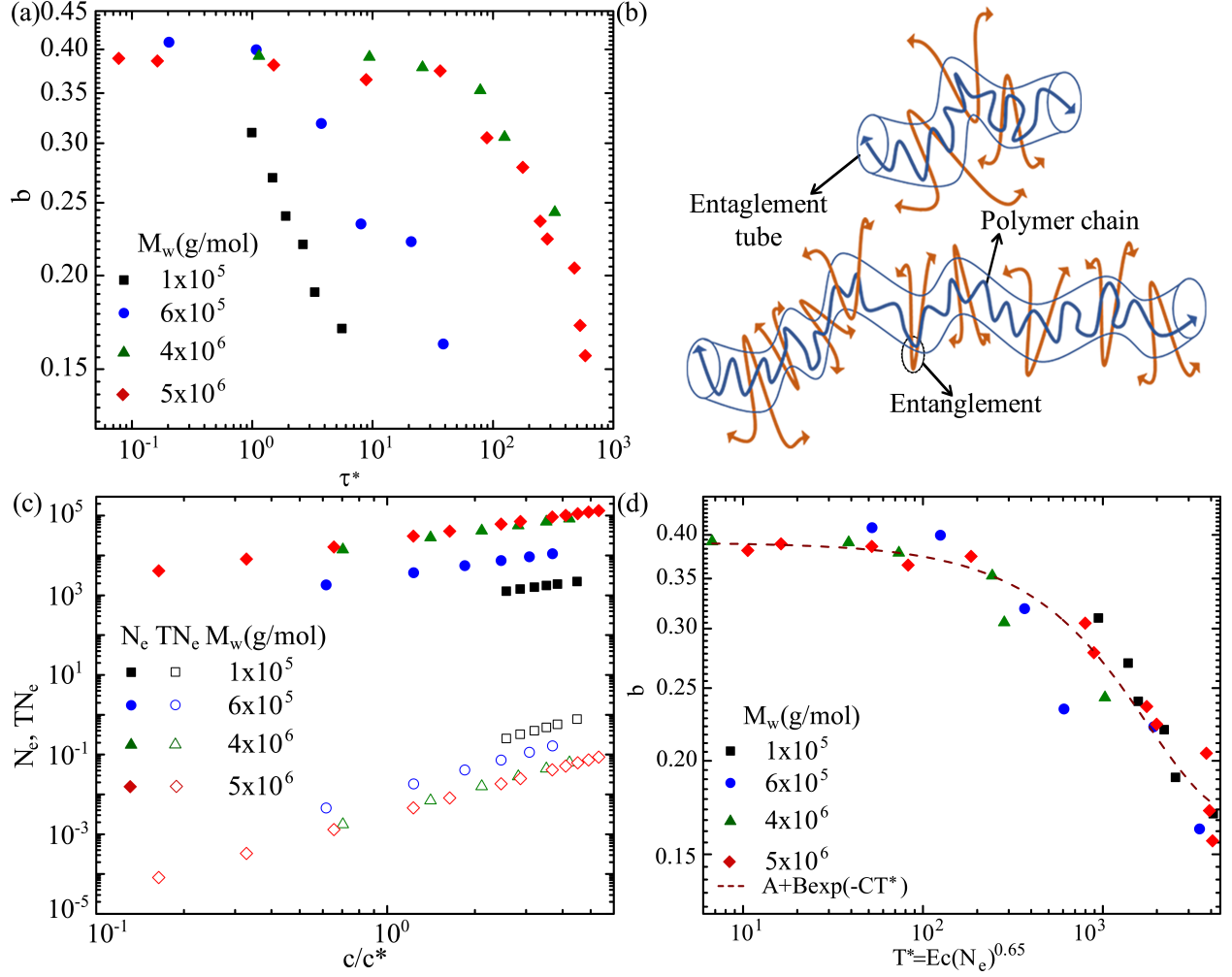


Figure 3: (a) Variation of b with the dimensionless time τ^* proposed in our previous study¹² across different molecular weights, (b) Schematic of the chain entanglements for two different chain lengths, (c) Dependence of entanglement density N_e and total entanglement density $TN_e = N_e \times N_d$ (N_d is the order of number of chains) on c/c^* across molecular weights and (d) Dependence of the power-law exponent b on T^* (ratio of τ_v and relaxation time λ) for various molecular weights. The dashed line represents the exponential fit of 94% confidence interval with $A = 0.1653 \pm 0.01532$, $B = 0.22545 \pm 0.01508$, and $C = 0.00076 \pm 0.00017$.

the data obtained from our previous study¹² for $M_w = 5 \times 10^6$ g/mol and $M_w = 4 \times 10^6$ g/mol is shown in Fig. 3(a). It is observed that there is a significant deviation in b vs τ^* for $M_w = 6 \times 10^5$ and $M_w = 1 \times 10^5$ g/mol compared to the other two molecular weights. This deviation is related to the macromolecular dynamics of the chains rather the continuum behaviour. Such dependence can be explained using the entanglement density i.e entanglement junctions per chain, $N_e = (\frac{M_w}{M_e})(\frac{c}{c^*})$,²⁷ where M_e is entanglement molecular weight, which is 2000

g/mol for PEO.²⁸ The N_e values for different c/c^* and M_w are given in Fig. 3(c). It can be observed from Fig. 3(c), the entanglement densities for same c/c^* across the molecular weights differ by an order between $M_w = 1 \times 10^5$, 6×10^5 g/mol and 5×10^6 g/mol. Whereas, for molecular weights of 4×10^6 g/mol and 5×10^6 g/mol, N_e are of same order. As N_e for $M_w = 1 \times 10^5$ and $M_w = 6 \times 10^5$ g/mol is less than the other two molecular weights, the chains have lesser topological constraints owing to the small chain lengths resulting in much lower relaxation times. The corresponding entanglement constrains for two different chain lengths is represented in Fig. 3(b) as a schematic. This difference in relaxation times is reflected in the continuum approach through the shear modulus $G = \eta_o/\lambda$. The G values corresponding to various c/c^* and M_w are given in Table-2. The difference in G for same c/c^* across the molecular weights suggests a stronger approach to solid like behaviour leading to a faster decrease in exponent b for $M_w = 1 \times 10^5$ and $M_w = 6 \times 10^5$ g/mol. This is further understood by the scale of total entanglement density $TN_e = N_e \times N_d$ where N_d is the scale of number of chains per unit volume. Fig. 3(c) shows that for the same c/c^* , TN_e increases as the M_w decreases indicating higher density of entanglement junctions per unit volume for lower M_w resulting in higher G at same c/c^* . As the coalescence process is an energy minimization phenomenon, the increase in G leads to increase in elastic energy per unit volume²⁹ $e = \frac{3}{2}G\epsilon^2$. Once this elastic energy predominates the surface energy, the coalescence is arrested. Such approach to arrested coalescence leads to faster decrease in b .

To account for the deviation of b with τ^* across molecular weights as represented in Fig. 3(a), we redefine the non-dimensional characteristic time as $T^* = \frac{\tau_w}{\lambda}(N_e)^{0.65} = Ec(N_e)^{0.65}$ (where, $\tau_w = \frac{\eta_o R_o}{\sigma}$). Here, $N_e^{0.65}$ is added empirically. This term accounts for the entanglement density which is the fingerprint of entanglement junctions in the continuum. Therefore, $T^* = Ec(N_e)^{0.65}$ is the corrected time scale to represent the behaviour of power-law exponent b . Such behaviour is represented in Fig. 3(d). Addition of N_e in T^* suggests that the continuum approach is not complete until the molecular description of chain dynamics via entanglement densities are empirically added to the continuum description. Similarly, c/c^*

was empirically added in the functional dependence of the scaling constants A_1 and A_2 with Ec to account for the entanglement densities. The collapse of data shown in Fig. 3(d) follows an exponential decay function similar to that in our previous study.¹²

Finally, we look at one of the limiting cases of Eq (10). For getting a physically acceptable solution, it is important to have non-negative sum under square-root. One such case that violates the condition is when $P = 0$ as the term Q is always negative. On substituting $P = 0$, we obtain Eq (11) that can be further simplified to obtain a cut-off radius in terms of material properties at which the coalescence is arrested. It is observed from Fig. 2(c), the value of the term $|\frac{A_1}{A_2}|$ is bounded by $\mathcal{O}(10)$. Under small angle limit $R = R_0\theta$ as represented in Fig. S3, Eq (11) is further simplified to obtain the θ_{arrest} (angle subtended by neck when coalescence is arrested) as represented in Eq (12).

$$-\frac{A_1}{A_2} = \frac{\frac{\eta}{\lambda} + \frac{2R_o}{R}}{\sigma\left(\frac{1}{R} + \frac{2R_o}{R^2}\right)} \quad (10)$$

$$\theta_{arrest} = \frac{4.47}{\sqrt{Ec}} \quad (11)$$

The proposed value for θ_{arrest} is in good agreement with the value proposed in literature for high elasticity droplets.³⁰ It is important to note that our result over predicts the value which we owe to experimental sensitivity and the stronger assumption of $P = 0$. To further validate θ_{arrest} given in Eq (12), experiments are performed on $c/c^* = 77$ of $M_w = 1 \times 10^5$ g/mol having the properties $\eta_o = 75$ Pa.s and $\lambda = 17$ ms. In the current study, we have considered coalescence as arrested if $\dot{\gamma}_{arrest} < 0.5\%(\dot{\gamma}_{DIwater})$, where $\dot{\gamma}$ is shear rate (See supplementary information for shear rate calculations). The value of θ_{arrest} obtained from experiments is 0.35 radians which is in agreement with the value obtained from Eq (12) i.e. 0.48 radians. This experimentally obtained θ_{arrest} is in between the values obtained from Eq (12) and the

relation proposed by Ongenae et al.³⁰ for the arrested coalescence. However, it is important to note that in sessile-pendant configuration, gravity becomes an important parameter at the higher time scales owing to which coalescence is no longer arrested.

Conclusion

In the current work, we have developed a theoretical framework to model polymeric droplet coalescence. We have unified the various constitutive laws under high Weissenberg creep flow limit to obtain a scaling based neck evolution equation. The theoretical framework is validated across different molecular weights of Poly(ethylene oxide) (PEO) with experiments. Our experiments and theoretical model have both highlighted the importance of macromolecular parameters for understanding the coalescence dynamics. The study also reports an empirically corrected T^* over our previous study to account for entanglement densities across different molecular weights. Theoretical framework is further validated by looking at a limiting case of arrested coalescence under small angle limit. The value we obtain for θ_{arrest} is found to be inversely proportional to $Ec^{1/2}$ and is validated with experiments along with the value proposed in literature. Finally, we name the coalescence as sub-Newtonian if $b < 0.5$ with limiting case $b \rightarrow 0$ as arrested. However, the current framework implicitly assumes Weber Number $We = (\rho U^2 R_o)/\sigma \rightarrow 0$ and neglects the effect of surrounding fluids by assuming low approach velocity and air as the outer fluid respectively. Further studies on different complex fluids are required to broaden the class of sub-Newtonian coalescence along with the effect of higher approach velocities and different surrounding fluids. It also poses an open question about the existence of super-Newtonian coalescence $b > 0.5$ where the merging dynamics will be driven by an additional force other than capillary and therefore will hasten the coalescence dynamics.

Materials and methods

Poly(ethylene oxide) (PEO) of molecular weight $M_w = 6 \times 10^5$ and 1×10^5 g/mol, solutions of various concentrations c are prepared by adding the sufficient quantity of polymer to DI Water. All the solutions are agitated at 300 rpm to ensure homogeneous dispersion. Concentrations are chosen such that the solutions are in semi-dilute entangled regime ($c > c_e$, where $c_e = 6c^*$ ³¹ is an entanglement concentration and c^* is the critical concentration). Critical concentration is obtained using the Mark-Houwink-Sakurada relation³² for PEO and Flory relation $c^* = \frac{1}{0.072M_w^{0.65}}$. For $M_w = 4 \times 10^6$ and 5×10^6 g/mol data is taken from our previous study.¹³ The corresponding values of critical concentration and entanglement concentration for the chosen polymers are given in Table-1. The concentrations and corresponding concentration ratios c/c^* of the solutions are given in Table-S1 along with the rheology data in supplementary information.

Table 1: List of molecular weights of polymers along with their critical and entanglement concentrations. (Note: * represents data obtained from Varma et al.¹³)

Polymer	M_w (g/mol)	c^* (% w/v)	c_e (% w/v)
PEO	1×10^5	0.781	4.686
PEO	6×10^5	0.244	1.464
PEO	* 4×10^6	0.061	0.366
PEO	* 5×10^6	0.071	0.426

Experiments are performed on a glass substrate coated with Polydimethylsiloxane (PDMS). Before coating the PDMS, substrates are cleansed with detergent followed by sonication with DI water and acetone for 20 mins each and later allowing them to dry in a hot air oven at 95°C for 30 mins. PDMS and the curing agent (Syl Gard 184 Silicone Elastomer Kit, Dow Corning) are mixed in 1:10 ratio through agitation. This mixture is desiccated for 30 mins to remove the visible bubbles in the solution. Finally, the PDMS substrates are obtained by dripping the mixture on glass substrate and spin coating at 5000 rpm for 60 s.

References

- (1) Frenkel, J. Viscous flow of crystalline bodies under the action of surface tension. *J. phys.* **1945**, *9*, 385.
- (2) Villermaux, E.; Bossa, B. Single-drop fragmentation determines size distribution of raindrops. *Nature Physics* **2009**, *5*, 697.
- (3) Pruppacher, H. R.; Klett, J. D. *Microphysics of Clouds and Precipitation*; Springer, 2010; pp 10–73.
- (4) Orme, M. Experiments on droplet collisions, bounce, coalescence and disruption. *Progress in Energy and Combustion Science* **1997**, *23*, 65–79.
- (5) Hopfes, T.; Petersen, J.; Wang, Z.; Giglmaier, M.; Adams, N. Secondary Atomization of Liquid Metal Droplets at Moderate Weber Numbers. *International Journal of Multiphase Flow* **2021**, *143*, 103723.
- (6) Stewart, S.; Mazza, G. EFFECT OF FLAXSEED GUM ON QUALITY AND STABILITY OF A MODEL SALAD DRESSING 1. *Journal of Food Quality* **2000**, *23*, 373–390.
- (7) Ashgriz, N.; Poo, J. Coalescence and separation in binary collisions of liquid drops. *Journal of Fluid Mechanics* **1990**, *221*, 183–204.
- (8) Djohari, H.; Martínez-Herrera, J. I.; Derby, J. J. Transport mechanisms and densification during sintering: I. Viscous flow versus vacancy diffusion. *Chemical Engineering Science* **2009**, *64*, 3799–3809.
- (9) Ambrose, J.; Livitz, M.; Wessels, D.; Kuhl, S.; Lusche, D. F.; Scherer, A.; Voss, E.; Soll, D. R. Mediated coalescence: a possible mechanism for tumor cellular heterogeneity. *American journal of cancer research* **2015**, *5*, 3485.

- (10) Varma, S. C.; Saha, A.; Mukherjee, S.; Bandopadhyay, A.; Kumar, A.; Chakraborty, S. Universality in coalescence of polymeric fluids. *Soft Matter* **2020**, *16*, 10921–10927.
- (11) Varma, S. C.; Saha, A.; Kumar, A. Coalescence of polymeric sessile drops on a partially wettable substrate. *Physics of Fluids* **2021**, *33*, 123101.
- (12) Varma, S. C.; Rajput, A. S.; Kumar, A. Rheocoalescence: Relaxation time through coalescence of droplets. *Macromolecules* **2022**,
- (13) Varma, S. C.; Dasgupta, D.; Kumar, A. Elasticity can affect droplet coalescence. *arXiv preprint arXiv:2205.11815* **2022**,
- (14) Chen, S.; Pirhadi, E.; Yong, X. Viscoelastic necking dynamics between attractive microgels. *Journal of Colloid and Interface Science* **2022**, *618*, 283–289.
- (15) Xu, H.; Wang, T.; Che, Z. Bridge evolution during the coalescence of immiscible droplets. *Journal of Colloid and Interface Science* **2022**,
- (16) Chen, H.; Pan, X.; Nie, Q.; Ma, Q.; Fang, H.; Yin, Z. Probing the coalescence of non-Newtonian droplets on a substrate. *Physics of Fluids* **2022**, *34*, 032109.
- (17) Thien, N. P.; Tanner, R. I. A new constitutive equation derived from network theory. *Journal of Non-Newtonian Fluid Mechanics* **1977**, *2*, 353–365.
- (18) Phan-Thien, N. A nonlinear network viscoelastic model. *Journal of Rheology* **1978**, *22*, 259–283.
- (19) Bird, R. B.; Armstrong, R. C.; Hassager, O. *Dynamics of polymeric liquids. Vol. 1, 2nd Ed. : Fluid mechanics*; Wiley, 1987.
- (20) Giesekus, H. A simple constitutive equation for polymer fluids based on the concept of deformation-dependent tensorial mobility. *Journal of Non-Newtonian Fluid Mechanics* **1982**, *11*, 69–109.

- (21) Renardy, M. The high Weissenberg number limit of the UCM model and the Euler equations. *Journal of non-newtonian fluid mechanics* **1997**, *69*, 293–301.
- (22) Bellehumeur, C. T.; Kontopoulou, M.; Vlachopoulos, J. The role of viscoelasticity in polymer sintering. *Rheologica acta* **1998**, *37*, 270–278.
- (23) Xia, X.; He, C.; Zhang, P. Universality in the viscous-to-inertial coalescence of liquid droplets. *Proceedings of the National Academy of Sciences* **2019**, *116*, 23467–23472.
- (24) Wu, M.; Cubaud, T.; Ho, C.-M. Scaling law in liquid drop coalescence driven by surface tension. *Physics of Fluids* **2004**, *16*, L51–L54.
- (25) Paulsen, J. D.; Burton, J. C.; Nagel, S. R. Viscous to inertial crossover in liquid drop coalescence. *Physical Review Letters* **2011**, *106*, 114501.
- (26) Sprakel, J.; van der Gucht, J.; Stuart, M. A. C.; Besseling, N. A. Brownian particles in transient polymer networks. *Physical Review E* **2008**, *77*, 061502.
- (27) Huang, Q.; Mednova, O.; Rasmussen, H. K.; Alvarez, N. J.; Skov, A. L.; Almdal, K.; Hassager, O. Concentrated polymer solutions are different from melts: Role of entanglement molecular weight. *Macromolecules* **2013**, *46*, 5026–5035.
- (28) Nath, P.; Mangal, R.; Kohle, F.; Choudhury, S.; Narayanan, S.; Wiesner, U.; Archer, L. A. Dynamics of nanoparticles in entangled polymer solutions. *Langmuir* **2018**, *34*, 241–249.
- (29) Pawar, A. B.; Caggioni, M.; Hartel, R. W.; Spicer, P. T. Arrested coalescence of viscoelastic droplets with internal microstructure. *Faraday discussions* **2012**, *158*, 341–350.
- (30) Ongenaes, S.; Cuvelier, M.; Vangheel, J.; Ramon, H.; Smeets, B. Activity-induced fluidization and arrested coalescence in fusion of cellular aggregates. *Frontiers in Physics* **2021**, 321.

- (31) Arnolds, O.; Buggisch, H.; Sachsenheimer, D.; Willenbacher, N. Capillary breakup extensional rheometry (CaBER) on semi-dilute and concentrated polyethyleneoxide (PEO) solutions. *Rheologica Acta* **2010**, *49*, 1207–1217.
- (32) Tirtaatmadja, V.; McKinley, G. H.; Cooper-White, J. J. Drop formation and breakup of low viscosity elastic fluids: Effects of molecular weight and concentration. *Physics of Fluids* **2006**, *18*, 043101.